Polymer 99 (2016) 671–683

Contents lists available at ScienceDirect

Polymer

journal homepage: www.elsevier.com/locate/polymer

4,4′-methylene diphenyl diisocyanate – Conformational space, normal vibrations and infrared spectra

Frank Fug [a, *], Kevin Rohe [b], Jorge Vargas [b, c], Christophe Nies [a], Michael Springborg [b, d], Wulff Possart [a]

[a] Adhesion and Interphases in Polymers, Saarland University, D-66123 Saarbrücken, Germany
[b] Physical and Theoretical Chemistry, Saarland University, D-66123 Saarbrücken, Germany
[c] Instituto de Investigaciones en Materiales, Universidad Nacional Autónoma de México, s/n A.P. 70-360, C.P. 04510 Ciudad de Mexico, Mexico
[d] School of Materials Science and Engineering, Tianjin University, Weijin Road, No. 92, Tianjin 300072, China

ARTICLE INFO

Article history:
Received 12 April 2016
Received in revised form
22 July 2016
Accepted 26 July 2016
Available online 28 July 2016

Keywords:
4,4′-methylene diphenyl diisocyanate (4,4′-MDI)
DFT calculations
Infrared spectroscopy

ABSTRACT

Though 4,4′-methylene diphenyl diisocyanate (4,4′-MDI) is a key monomer in polyurethane synthesis, its infrared spectrum has not been discovered and assigned to the molecular vibrations in detail yet. To close that impedimental analytical gap, the conformers of 4,4′-MDI and their vibrational properties are explored by DFT calculations and accurate IR band assignment is achieved for the first time by detailed comparison with measured spectra. Eight conformers are identified for 4,4′-MDI. They can be separated into three classes with distinct physical and/or chemical properties. The classes differ in energy of the molecule and in the orientation of the isocyanate groups. For comparison with the IR spectrum measured for gaseous 4,4′-MDI, the conformer spectra are broadened with Lorentzians, weighted according to the Boltzmann distribution for the conformer states, and added. This cumulated 4,4′-MDI spectrum does not possess conformation-sensitive bands and differs significantly from the gas phase IR spectrum: IR bands are not related to the normal vibrations on a one-to-one basis since more than one normal mode contributes to each IR band. The IR normal modes show for all conformers that nearly all atoms are involved in each vibration. Moreover, spectra comparison reveals various significant differences that indicate that intermolecular interactions affect the measured spectra for the liquid and the gas state as well.

1. Introduction

Infrared spectroscopy serves as a powerful characterization method for chemical substances. Absorption of electromagnetic energy at the vibration eigenfrequencies in the sample results in a spectrum of IR bands which are assigned to the chemical structure of the molecule. A closer look to the IR spectra of the majority of organic molecules reveals fewer bands than eigenvibrations. Hence the bands result from some superposition of molecular vibrations.

In addition, band assignment is generally performed with the help of band catalogues [1–4]. These are based on spectra measured in the mid infrared frequency region (MIR) for very many well-defined model samples. The catalogues for organic molecules are based on the phenomenological observation that the so-called characteristic IR bands can be assigned to specific functional groups, i.e. to a limited number of specified atoms of the molecule. This concept is referred to as a ‘group frequency approach’. Sometimes this approach is extended to the idea that the given characteristic mid IR absorption band results from the vibration of just this specific atom group, and some authors attribute the characteristic group frequency to a ‘local mode’ (cf. e.g. Ref. [5]). Eigenvibrations of molecules, however, are localized only in very exceptional cases (e.g. for MIR vibrations of light hydrogen atoms bonded to much heavier atoms like carbon or in the near infrared region for special overtone vibrations in some molecules which then are rightly called ‘local modes’). Instead, large parts of the molecule or even all atoms contribute to most vibrational modes. Owing to varying intra- and intermolecular environment in the model samples, a *frequency range* is assigned to a given functional group in the catalogues instead of the sharp frequency it must have in any given situation. Hence, in many cases it is essentially impossible to determine exactly which groups or parts of the

* Corresponding author.
E-mail address: f.fug@mx.uni-saarland.de (F. Fug).

http://dx.doi.org/10.1016/j.polymer.2016.07.075
0032-3861/

molecule contribute to a given IR band. Last not least unusual molecules are missing in the catalogues. Sophisticated molecular modelling provides a way out of all these dilemmas.

4,4′-Methylene diphenylene diisocyanate (4,4′-MDI, cf. Fig. 1) is one of the molecules lacking precise IR band assignment.

4,4′-MDI is a key component for polyurethane (PU) synthesis via polyaddition to polyols – Fig. 2. The properties of PU polymers are mainly adjusted by varying the polyol component as only few isocyanates meet application demands. In that sense a detailed band assignment for the isocyanate molecule is of fundamental importance for proper characterization.

Based on quantum mechanical density-functional theory (DFT) simulations, this paper analyses the conformational states of 4,4′-MDI and their effect on the IR spectra with respect to frequency, intensity and transition dipole moment. As the 4,4′-MDI molecule contains only four C-X sigma bonds with X being C or N, few rotational degrees of freedom exist for the functional isocyanate groups. A reference IR spectrum of pure 4,4′-MDI measured in the gas phase shall serve as benchmark for the accuracy of the calculations.

2. Methods

2.1. Experimental methods

4,4′-methylene diphenyl diisocyanate (≥99.5%, Acros Organics) is evaporated at ca. 220 °C under nitrogen atmosphere. With the carrier gas, the vapour streams at ca. 200 °C through a gas transmission cell of a FTIR spectrometer (spectral resolution: 4 cm^{-1}, Tensor 27, Bruker, Ettlingen, Germany). As a second approach, super-cooled liquid 4,4′-MDI is measured at room temperature with IR-ATR (attenuated total reflection) using a ZnSe hemisphere as ATR element and *p*-polarised light at 60° angle of incidence and 4 cm^{-1} spectral resolution.

It has to be emphasised that the transmission and the ATR spectrum must not be compared directly as the optical set-up affects the measured spectrum. To solve that issue a suitable transformation of both transmission and ATR spectrum has to be developed. In IR spectroscopy two single beam spectra are measured: the 'background' spectrum (BKG) for the empty spectrometer and the 'sample' spectrum (SAM) with the sample. Except for experimental noise, the division of these single beam spectra cancels all factors from the spectrometer and results in the pure spectrum of the sample. Lambert's law applies for transmission spectra and both BKG and SAM spectrum are given as:

$$I_{BKG}(\tilde{\nu},z) = I_0(\tilde{\nu})\cdot e^{-4\pi\tilde{\nu}zK_{BKG}(\tilde{\nu})} \tag{1}$$

$$I_{SAM}(\tilde{\nu},z) = I_0(\tilde{\nu})\cdot e^{-4\pi\tilde{\nu}z(K_{BKG}(\tilde{\nu})+K_{SAM}(\tilde{\nu}))} \tag{2}$$

with I: measured intensity.I_0: initial intensity of the IR light source.$\tilde{\nu}$: wave number. z: optical path length in the set-up. K: extinction index as part of the optical function.

$$n^*(\tilde{\nu}) = n(\tilde{\nu}) + i\cdot K(\tilde{\nu}) \tag{3}$$

The transmittance spectrum $T_{SAM}(\tilde{\nu})$ for the sample is obtained as

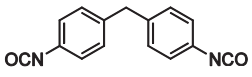

Fig. 1. Chemical structure of the 4,4′-methylene diphenyl diisocyanate.

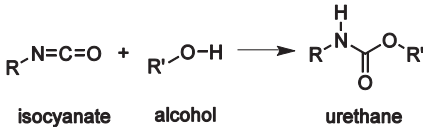

Fig. 2. Formation of urethane by addition of an alcohol to an isocyanate.

$$T_{SAM}(\tilde{\nu}) = \frac{I_{SAM}}{I_{BKG}} = \frac{e^{-4\pi\tilde{\nu}z(K_{BKG}(\tilde{\nu})+K_{SAM}(\tilde{\nu}))}}{e^{-4\pi\tilde{\nu}zK_{BKG}(\tilde{\nu})}} = e^{-4\pi\tilde{\nu}zK_{SAM}(\tilde{\nu})} \tag{4a}$$

or

$$\ln T_{SAM}(\tilde{\nu}) = -4\pi\tilde{\nu}zK_{SAM}(\tilde{\nu}). \tag{4b}$$

Given the optical path length *z*, the absorption index function $K_{SAM}(\tilde{\nu})$ follows as the information on light absorption characteristics of the sample material. In case that *z* is not known exactly, a band at a given wavenumber $\tilde{\nu}_{ref}$ is chosen as internal reference for normalization. Similar to eq. (1) and (2) Lambert's law gives for $\tilde{\nu}_{ref}$

$$I_{BKG}\left(\tilde{\nu}_{ref},z\right) = I_0\left(\tilde{\nu}_{ref}\right)\cdot e^{-4\pi\tilde{\nu}_{ref}zK_{BKG}\left(\tilde{\nu}_{ref}\right)} \tag{5}$$

$$I_{SAM}\left(\tilde{\nu}_{ref},z\right) = I_0\left(\tilde{\nu}_{ref}\right)\cdot e^{-4\pi\tilde{\nu}_{ref}z\left(K_{BKG}\left(\tilde{\nu}_{ref}\right)+K^{ref}_{SAM}\left(\tilde{\nu}_{ref}\right)\right)} \tag{6}$$

and the transmittance spectrum for the reference band is calculated as

$$T_{ref}\left(\tilde{\nu}_{ref}\right) = \frac{I^{ref}_{SAM}\left(\tilde{\nu}_{ref}\right)}{I_{BKG}\left(\tilde{\nu}_{ref}\right)} = e^{-4\pi\tilde{\nu}_{ref}zK^{ref}_{SAM}\left(\tilde{\nu}_{ref}\right)} \tag{7a}$$

$$\ln T_{ref}\left(\tilde{\nu}_{ref}\right) = -4\pi\tilde{\nu}_{ref}zK^{ref}_{SAM}\left(\tilde{\nu}_{ref}\right) \tag{7b}$$

Now, the normalization is carried out by dividing eq. (4b) by eq. (7b)

$$\frac{\ln T_{SAM}(\tilde{\nu})}{\ln T_{ref}\left(\tilde{\nu}_{ref}\right)} = \frac{\tilde{\nu}\cdot K_{SAM}(\tilde{\nu})}{\tilde{\nu}_{ref}\cdot K^{ref}_{SAM}\left(\tilde{\nu}_{ref}\right)} \tag{8}$$

The left-hand-side of eq. (8) is easily calculated from the measured transmittance spectrum. On the right-hand side the optical path length disappeared but the sample absorption index function, $K_{SAM}(\tilde{\nu})$ can be derived only with a known value for $K^{ref}_{SAM}(\tilde{\nu}_{ref})$.

Here the ATR spectrum comes into play. It contains the IR optical function $n^*_{SAM}(\tilde{\nu})$ of the sample material and hence $K_{SAM}(\tilde{\nu})$ which is deduced with an appropriate software (eg. software package FSOS [6]). The software implements the Kramers-Kronig transformation [7–10], accounts for the effects of the optical configuration on the spectrum, and for the penetration depth of the evanescent wave in ATR which depends on $\tilde{\nu}$ in a complex way.

Now, eq. (8) can be utilised for comparing the measured gas phase IR spectrum with the spectrum $K_{SAM}(\tilde{\nu})$ as derived from the ATR spectrum for the condensed phase of the sample material. For the 4,4′-MDI studied here we can check for stability against thermal evaporation and for differences in intermolecular interactions in the vapour versus liquid state.

2.2. Theoretical methods

All theoretical calculations are performed within the quantum mechanical density-functional theory as implemented in GAUS-

SIAN09 [11]. 13 basis sets of increasing size using B3LYP [12,13] or PBE functionals (Perdew-Burke-Ernzerhof [14] parameterization for the XC-potential) are tested. The results for the total energy, molecular structure, dipole moment, eigenvibration and corresponding IR spectra are compared. IR spectra calculated with the PBE functional, match the experimental gas phase spectrum better than those obtained with B3LYP. The 6-31 + G(d) basis set is the smallest one among the basis sets which produce reasonable agreement of vibrational frequencies with IR band positions in the gas phase spectrum of 4,4′-MDI. Although more sophisticated basis sets are feasible, the 6-31 + G(d) set was chosen for all calculations presented in this paper as it will enable the simulation for a monomer adsorbed on a solid in a forthcoming study where bigger basis sets would significantly increase the calculation effort. Only after full structural optimization, the normal modes with their vibrational frequencies and IR intensities are obtained with the harmonic approximation in a subsequent calculation. The calculated IR intensities depend on the derivatives of the molecular dipole moment with respect to the normal coordinates and since calculated dipole moments often only then are accurately reproduced when large basis sets are used in the calculations, these intensities are related with some uncertainties.

3. Results and discussion

3.1. Experimental IR spectra: gaseous versus liquid 4,4′-MDI

A high quality of the measured gas phase transmission spectrum of 4,4′-MDI is of major importance because it shall serve as benchmark for the quantum mechanical results. Therefore, eq. (8) is utilised for a comparison with $K_{SAM}(\tilde{\nu})$ as derived from the ATR spectrum of liquid 4,4′-MDI. The sharp and isolated band at $\tilde{\nu}_{ref}$ = 1019 cm^{-1} is chosen as the reference. Fig. 3a depicts the complete IR spectra while Fig. 3b–d shows close-up views of each spectral region.

Besides the peak at 2356 cm^{-1} which is irrelevant as it indicates some residual CO_2 in the gas phase, the 'bands' possess a number of different features in both 'spectra'. The intense band at 2280 cm^{-1} (mainly due to a NCO stretch vibration) is more intense and has wider tails in the gas than in the liquid. A close look indicates that except for the range 3200 cm^{-1} - 2800 cm^{-1}, all bands are slightly sharper in the liquid spectrum. This observation surprises since one would expect the opposite for the band width. It should be quite small in the gas phase as molecules are well separated while intermolecular interactions should cause band broadening in the dense liquid state. In the region of 1800–1400 cm^{-1}, the bands appear at equal positions in both spectra and possess similar width but the relative intensity varies for some bands. At 1300–1100 cm^{-1} (marked as '1' in Fig. 3d) the relative intensities are different and bands in the gas phase shift slightly to higher wavenumbers (by ca. 20 cm^{-1}). That is relevant with respect to the given spectral resolution of 4 cm^{-1}. In region '2' (900–750 cm^{-1}) we see a doublet in the liquid state while the low-frequency peak reduces to a shoulder in the gas phase spectrum. All these distinctions between both spectra are mainly attributed to a different specificity of intermolecular interactions in the produced vapour and in the liquid state. They reveal the spectral regions where these interactions give the most notable changes in the IR spectra. Various intermolecular interactions are present even in the measured vapour. A lower 4,4′-MDI vapour density would reduce the effects but, simultaneously, the intensity and, therefore, the quality of the measured IR spectrum. In conclusion, the recorded gas phase spectrum agrees reasonably well with the spectrum of the liquid. Particularly, it does not reveal any deterioration due to thermal evaporation and may serve for semi-quantitative comparison with the calculated spectra below.

3.2. Conformational space of 4,4′-MDI

A methylene group and two phenylene rings form the core of the 4,4′-MDI molecule. To each phenylene ring, an isocyanate group (NCO) is attached at the para position (opposite to the methylene). Fig. 4 shows the fully optimized molecule and introduces the notation we shall use for describing the geometry.

The carbon atoms 1, 2 and 5 define the plane of the molecule (POM) and span the angle $\beta = 114.6°$, i.e. a value close to the ideal value for sp^3-hybridised carbon atoms. The axis of the molecule (AOM), the carbons 8, 13, and the nitrogen atoms 24 and 27 all lie roughly in the POM. Due to the sp^2 hybridization of the nitrogen atoms, the angle $\angle CNC \equiv \alpha$ is 139.8° and the isocyanate atoms are in-plane with the adjacent phenylene ring (sketched in bluish grey in Fig. 4). Both phenylene rings are twisted by equal angles, $\psi_1 = \psi_2 = 55°$ with respect to the POM but in opposite directions. To be precise, ψ_1 and ψ_2 are the dihedral angles formed by the atoms 1, 2, 5, 6 and 5, 2, 1, 11, respectively (cf. Fig. 4).

In order to evaluate the structural flexibility and to search for the conformers, the energy landscape is scanned by rotating the phenylene rings together with their attached isocyanate group. ψ_1 and ψ_2 were varied in steps of 10° in the range (−90° … 270°) and (0° … 360°) respectively, with 0° corresponding to the phenylene ring in the POM. The rotation is done clockwise when looking from the methylene group towards the isocyanate. Initially the NCO groups are positioned in the plane of their corresponding phenylene ring (cf. Fig. 5).

The energy map as function of (ψ_1, ψ_2) was calculated as follows. At first, a total of eight local energy minima were identified. The corresponding molecule structures are the so-called conformers. Subsequently, for scanning the (ψ_1, ψ_2) beyond those energy minima, we fixed all other structural values at those for the structurally closest total-energy minimum. That provides an idea of the shape of the energy map offside the conformations. Fig. 6 presents the result as a function of dihedral angles ψ_1 and ψ_2. The six energy maxima (of which only four are different) correspond to cases where both phenylene rings lie in the POM. In this situation, one of the hydrogen atoms 16 and 19 is so close to one of the hydrogen atoms 20 and 23 that they repel each other resulting in a drastic increase of the total energy. On the other hand, for one phenylene perpendicular to the POM, the rotation of the other phenylene causes almost no change in the total energy (two dashed black lines at 90° in Fig. 6b) Avoiding the six maxima and their neighbourhood, the remaining energy barriers are lower than 0.1 eV.

A closer look into the valleys reveals the eight shallow energy minima (shaded in light blue in Fig. 6a) – the conformers **A** to **H** of the 4,4′-MDI. Their optimised positions are shown in Fig 6b (red dots). Table 1 gives the angles (α, β, ψ_1 and ψ_2), dipole moment, μ, and energy difference, $E - E_E$, of all relaxed conformer structures. The four angles are described in Fig. 4. The values of the angles, dipole moment and energy, E, are directly provided by GAUSSIAN for each conformer. Fig. 7 depicts the molecular geometry of conformers **A** - **D** for illustration.

Accordingly, the conformers **A**, **D**, **F** and **G** possess the same dipole moment but a slight energy difference of 0.06 meV. In addition, conformers **B**, **E** and **C**, **H**, respectively, form pairs with similar dipole moments and energies. Thus, are these slight parameter variations among the conformers real or do they originate from numerical inaccuracies? Symmetry arguments help to answer that question.

If it is possible to pass from one conformer to another one by only rigid body rotation of the whole molecule (i.e. without any

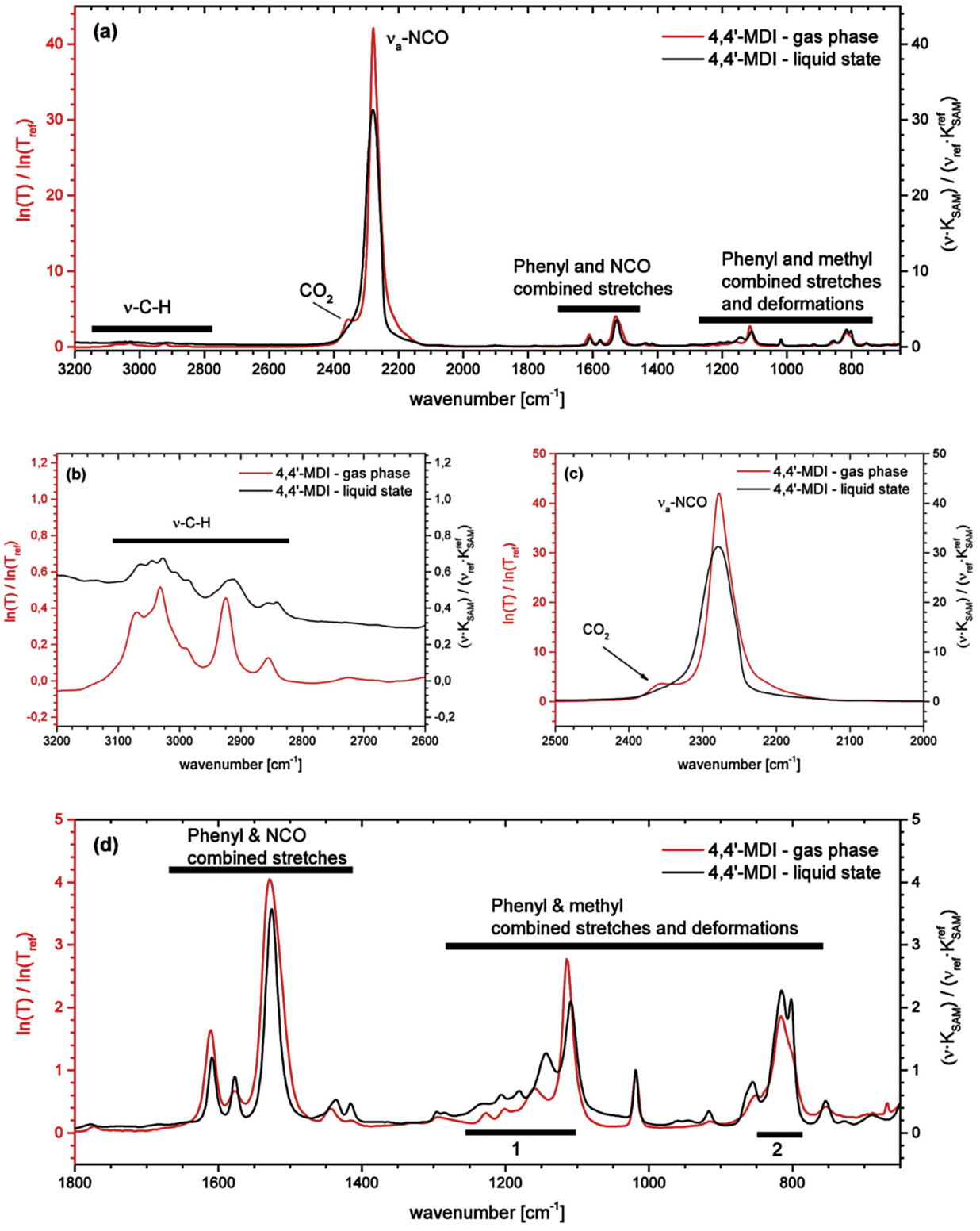

Fig. 3. Spectral distributions of $\ln T/\ln T_{ref}$ from a gas phase transmission spectrum (red) and of $(\tilde{\nu}\cdot K_{SAM})/(\tilde{\nu}_{ref}\cdot K^{ref}_{SAM})$ (black) as calculated from the extinction index spectrum in the liquid state of 4,4′-MDI. Complete spectrum (a) and close-up views (b–d). More details on bands are given in Table 4. (For interpretation of the references to colour in this figure legend, the reader is referred to the web version of this article.)

change of internal atom co-ordinates) then these conformers are identical and must have the same energy and dipole moment. Now, conformer **A** can be rotated to conformer **G**. Similarly **F** is obtained by rotation of **D**. Thus **A** is identical to **G** and **D** is identical to **F**. In other words, conformer pairs **A/G** and **D/F** are related through a C_2 operation. A look at their geometries shows that conformers **E** to **H** can be transformed into conformers **A** to **D** by a mirror operation in a plane parallel to the POM, so that for the energy and the dipole

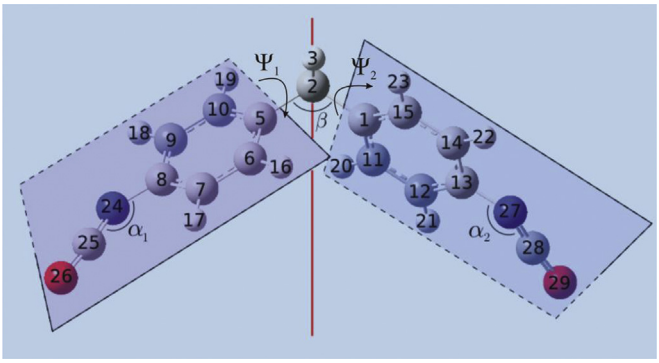

Fig. 4. Optimized spatial structure of the isolated 4,4′-MDI molecule. Oxygen: red, nitrogen: blue, carbon: grey and big, hydrogen: grey and small. Each of the isocyanate groups is in plane with its vicinal phenylene ring (bluish grey planes). We define the plane of the molecule (POM, cyan, in the plane of projection) by the carbon atoms 1, 2 and 5. They span the angle β, whose bisector is chosen as the axis of the molecule (AOM − red line, in the POM). Additionally, ψ_1 and ψ_2 are the dihedral angles formed by the carbons 1, 2, 5, 6 and 5, 2, 1, 11, respectively.

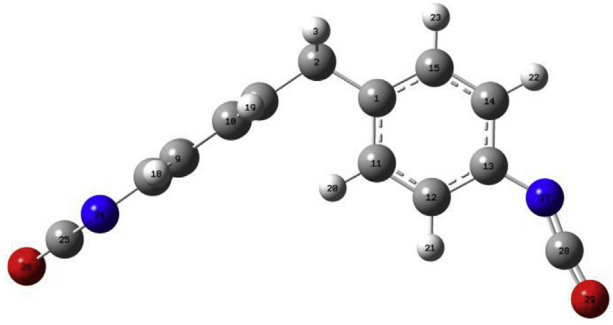

Fig. 5. Starting geometry for the energy landscape evaluation. $\Psi_1 = -90°$ and $\Psi_2 = 0°$. The left isocyanate group points behind the paper plane.

moment, **A** = **F**, **B** = **E**, **C** = **H** and **D** = **G**. The fact that the data in Table 1 do not completely match these conclusions is due to the shallowness of the total-energy landscape as shown in Fig. 6. The variations in the values can hence be taken as a measure for the accuracy of our reported data. For later purposes, we add that the two structures **B** and **C** possess a C_2 symmetry which is only approximately the case for conformer **A**, for which the different positions of the isocyanate groups disturb this symmetry.

Ultimately, the initial eight conformational states group in three distinct classes **I**, **II** and **III** (Table 2).

First, in any conformation, the phenylene rings are neither perpendicular ($\psi_i = 90°$) nor parallel ($\psi_i = 0°$) to the POM but tilted. For all eight conformations, the isocyanate group remains *in the plane* of the adjacent phenylene ring. However, the conformations differ in orientation of the rings/isocyanates with respect to the POM. A closer look reveals that both phenylene rings are always tilted on opposite sides of the POM. From the top view the isocyanates are either located at the same side of the POM (conformer class **I**, with conformer **A** as a representative) or on opposite sides (classes **II** and **III** with conformers **B** and **C**, respectively). Second, relaxation of the 4,4′-MDI molecule at any combination of the two ψ's always results in a conformer of one of the three classes.

For conformers **B** and **C** the total dipole moments are almost along with the AOM. The dipole moment vector of conformer **A** is slightly tilted with respect to the AOM as illustrated in Fig. 7.

The energy differences between the conformers are quite small but their dipole moments vary significantly. That originates from the different orientations of the NCO groups that provide a significant contribution to the total dipole moment. Accordingly, varying the angle between the NCO groups will considerably affect the resulting dipole moment of the whole molecule. For instance for conformer **C**, the large angles between the isocyanate groups and the AOM minimize the dipole moment of the 4,4′-MDI, which is accompanied by a rise in total energy.

A possible low-energy path from one conformation to the next is sketched as red line in Fig. 6b. A more detailed energy profile along this path was determined by rotating both phenylene rings (with NCO constantly aligned in the ring plane!) simultaneously by the same angle increment in 8 steps from the stable to the transition geometry (located at $\psi_2 = 90°$) where the red line crosses the black dashed ones in Fig. 6b. The result is shown as black curve in Fig. 8. The energy barrier between the conformer **B** and each of the other three is roughly 35 meV which is only slightly above the average thermal energy at room temperature (~26 meV).

Another process that may lead from one conformer to another consists in the rotation of just one of the two isocyanate groups,

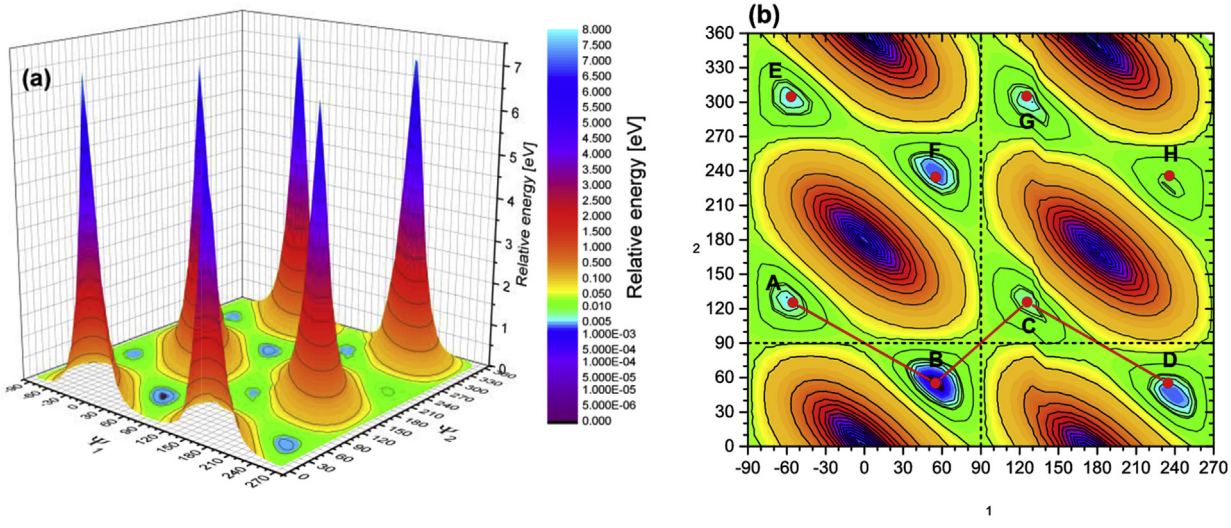

Fig. 6. Cavalier perspective (a) and top view (b) of the energy surface generated by the rotation of the phenylene rings keeping their bonded isocyanates in the plane of the ring. The eight energy-optimized conformers are indicated by the capitals **A** − **H** and the red dots in (b) for the shallow energy minima, as well as the optimal path (red) connecting **A**, **B**, **C** and **D**.

Table 1
Parameters of the eight 4,4′-MDI conformers as optimized with PBE/6−31 + g(d). The conformation **E** is chosen as reference for the energy difference.

Conformer	∠CNC angle $\alpha \approx \alpha_1 \approx \alpha_2$	Methylene angle β	*Dihedral angle* ψ_1	*Dihedral angle* ψ_2	Dipole moment μ	Relative energy $E - E_E$
	(Degree)				(Debye)	(meV)
A	138.8	114.5	−55.2	125.4	2.827	+1.88
B	139.8	114.5	55.0	55.0	3.072	0.20
C	139.9	114.6	125.7	125.7	2.464	+3.49
D	138.8	114.5	234.6	55.2	2.827	+1.88
E	139.9	114.2	−56.7	304.7	3.086	0
F	139.8	114.5	55.2	234.6	2.827	+1.82
G	139.9	114.5	125.4	305.2	2.827	+1.82
H	139.9	114.6	235.7	235.8	2.464	+3.53

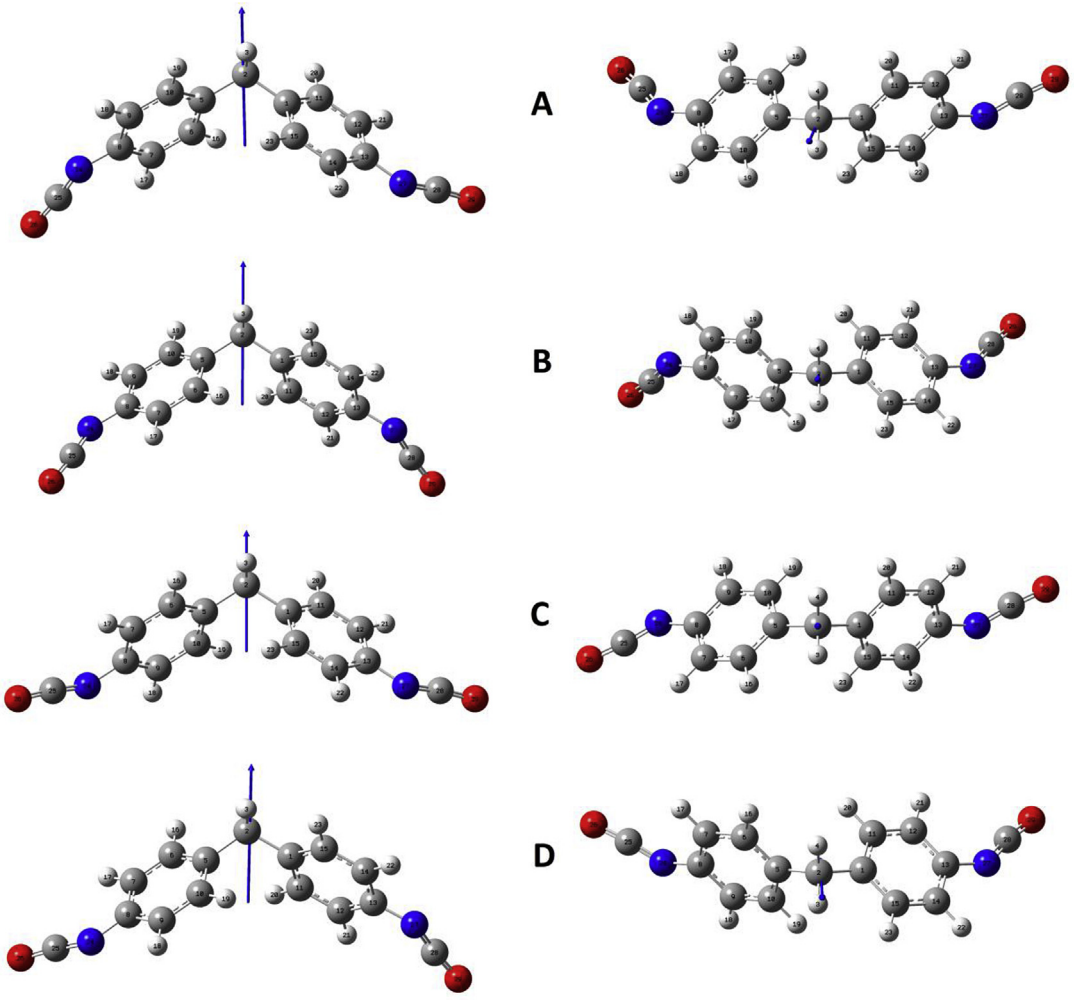

Fig. 7. The three conformers **A** - **C** of 4,4′-MDI with different physico-chemical properties and conformer **D** for comparison (left column: side view; right column: top view). **A** at $\psi_1 = -55.2°$ & $\psi_2 = 125.4°$, **B** at $\psi_1 = 55.0°$ & $\psi_2 = 55.0°$, **C** at $\psi_1 = 125.7°$ & $\psi_2 = 125.7°$, and **D** at $\psi_1 = 234.6°$ & $\psi_2 = 55.2°$. The blue arrows represent the corresponding dipole moment.

Table 2
Dipole moment and energy level of the three classes of 4,4′-MDI conformers. Conformer **E** is chosen as reference for the energy scale.

Conformer class	Dipole moment μ	Relative energy $E - E_E$
	(Debye)	(meV)
I: (A = D) = (F = G)	2.827	+1.88
II: B = E	3.086	0
III: C = H	2.464	+3.53

without rotating the phenylene rings. To study this, we changed the dihedral angle γ (defined by the atoms 12, 13, 27 and 28, cf. Fig. 4) from 0° (corresponding to the stable structure) to 90° (the transition structure) in steps of 10° starting from the relaxed structures. Fig. 8 compares the result (red and blue curves) with the energy profile obtained by varying the ψ angles of the phenylene groups with fixed NCO. The energy maximum corresponds to the perpendicular orientation of the isocyanate group with respect to the phenylene ring ($\gamma = 90°$). Rotation of the isocyanate group requires roughly twice the energy (~77 meV) needed for the rotation

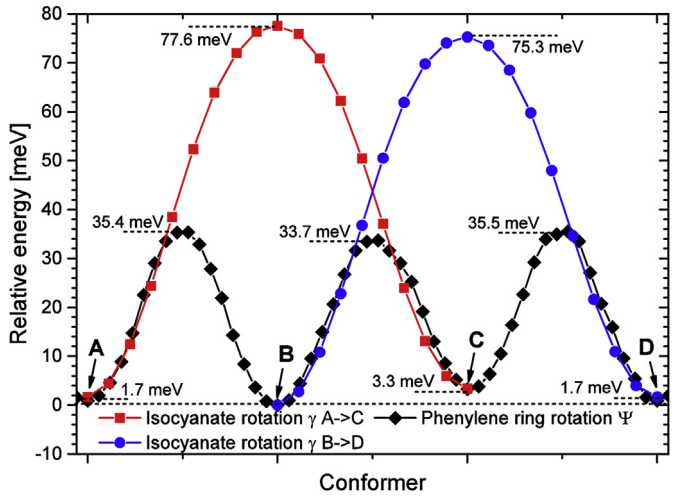

Fig. 8. Total energy of the 4,4′-MDI with respect to the conformer **B** when passing from one conformer to the other by rotating both phenylenes simultaneously (◆, along the red path shown in Fig. 6b) or by rotating only one isocyanate group (■ and ●, respectively). (For interpretation of the references to colour in this figure legend, the reader is referred to the web version of this article.)

of the phenylene groups (~35 meV). Thus, cooperative rotation of both phenylene rings is favoured for conformer transitions while each NCO group prefers to remain in the plane of 'its' pendant phenylene ring.

Since the conformational transition energy is in the range of thermal energy at room temperature, all conformers are present in a real sample. According to the Boltzmann distribution, the probability, p_j to find the conformer j with energy E_j at given absolute temperature, T is given by

$$p_j = \frac{N_j}{N} = \frac{e^{-\beta \cdot E_j}}{\sum_{k=1}^{8} e^{-\beta \cdot E_k}} = \frac{e^{-\beta \cdot E_j}}{Z} \tag{9}$$

$\beta = 1/kT$, k: Boltzmann constant.Z: partition function.

In our case, the sum consists of eight terms as eight conformers (Fig. 6) have to be considered in the distribution according to literature [15,16]. Conformers that can be transformed into other conformers using rigid body motions and mirror planes have the same spatial arrangement of atoms around the centre of the molecule and thus identical energy level and dipole moment. However, such conformers cannot be distinguished with IR spectroscopy. Hence these conformers can be grouped in a class (cf. Table 2) and their respective probabilities added.

Table 3 summarizes the probabilities obtained at room temperature.

With this distribution, we get 2.8 Debye for the average dipole moment which is in excellent agreement with the only experimental value of 2.75 Debye found in literature [17]. That gives a first proof of quality of the calculated molecule properties.

Table 3
Energies, E_j, and probabilities, p_j, of the Boltzmann distribution for the 4,4′-MDI conformers at 298 K.

Conformer	Energy $E_j - E_E$ (meV)	Probability p_j	Cumulated probability
A	1.88	0.125	0.50
D	1.88	0.125	
F	1.88	0.125	
G	1.88	0.125	
B	0	0.134	0.27
E	0	0.134	
C	3.53	0.117	0.23
H	3.53	0.117	

Next, the IR eigenvibration spectrum is calculated for each conformer. Quality and consistency of these spectra will be discussed in comparison with an IR spectrum measured for the 4,4′-MDI vapour. The experimental gas phase IR spectrum represents the superposition of the IR spectra of the conformers with the cumulated probabilities of Table 3 as the corresponding weight factors in a spectra simulation.

3.3. Modelling of infrared eigenvibration spectra for the 4,4′-MDI conformers

Quantum-mechanical modelling is a key tool for IR absorption band assignment in experimental IR spectra as it provides not only the frequencies of the normal vibration modes but also the infrared intensities which are closely related to the related transition dipole moments. Due to computational limitations, such simulations are, in most cases as well as in the following, restricted to one isolated molecule in vacuum. The 4,4′-MDI molecule has 81 normal modes of vibration, each one described by its eigenfrequency and IR absorption intensity (calculated using a harmonic approximation). In a first step, we calculate the eigenvibrations of conformer **B** (the representative of conformer class **II**) using the GAUSSIAN09 programs. Only part of the eigenvibrations falls into the typical mid IR range from 4000 to 400 cm^{-1}. As the region below 600 cm^{-1} is not covered properly in the IR spectroscopic measurement, only the range from 3200 to 650 cm^{-1} is discussed in this study. This mid IR part of the eigenvibration spectrum is presented as lines in Fig. 9.

Measured IR spectra show natural line broadening. In the gas phase, the natural line shape is well described by a Lorentz line, $g_i(x)$ with maximum intensity, I_i, and wave number, $\tilde{\nu}_i$, for each eigenvalue i

$$g_i(x) = \frac{\lambda_i^2 \cdot I_i}{(x - \tilde{\nu}_i)^2 + \lambda_i^2} \tag{10}$$

The parameter λ_i describes the width of the Lorentzian. Now, natural line broadening is taken into account by assigning a Lorentz line to each eigenvibration. This modified spectrum gives an idea of how eigenvibrations superimpose to the IR bands in the measured spectrum and provides accordingly the platform for IR band assignment. Since there is no general rule for choosing the line width, an arbitrary value of $\lambda = 10$ cm^{-1} is taken for all eigenvibrations in our calculated spectra. Note that the line widths of the calculated spectra therefore must not be compared to band widths in the measured gas spectrum.

The calculated spectrum of conformer **B** is presented in Fig. 9. This conformer, as conformer **C**, possesses C_2 symmetry and therefore for any vibrational mode, the displacements of symmetrically equivalent atoms will be identical. Thus, of symmetry reasons hardly any vibrational mode is localized to a single part of the molecule. Reducing the symmetry slightly, as is the case when passing to the **A** conformer, the vibrational modes will still be distributed almost equally among atoms that are almost symmetrically equivalent. Next, we shall discuss the vibrational spectrum in Fig. 9 in more detail. The region from 3200 to 2800 cm^{-1} (Fig. 9a) covers vibrations which are strongly localized to the CH-pairs (due to the low mass of hydrogen) and are well described as a stretch of the C—H bond. As shown below, such strong localisation is not the rule for eigenvibrations in organic molecules. The IR bands marked by '#1' are formed by the eight C—H stretch motions in the phenylene rings and the bands '#2' contain the two C—H stretching modes of the methylene group. Obviously, these IR bands are

Table 4
IR bands with wavenumber in cm^{-1} at peak maximum, calculated normal vibrations per band and dominating atom group motions for conformer **B** of 4,4′-MDI. Strong vibrations in **bold**, weak in *italics*.

IR band number	Wavenumber at peak	Normal vibrations in the band	Groups dominating the vibration mode
#7	1448	1452	Phenyl, **methyl**, NCO
		1450	**Phenyl**, *methyl*, **NCO**
		1444	Phenyl, **methyl**, *NCO*
#8	1418	1419	Phenyl, methyl
		1418	
#8	1418	1419	Phenyl, methyl
		1418	
#9	1353	1356	Phenyl, **methyl**
		1353	
#10	1299	1304	Phenyl, methyl
		1297	
	1278	1277	Phenyl, methyl
#11	1200	1201	Phenyl, methyl
		1190	
	1176	1179	Phenyl, methyl
		1177	Phenyl, *methyl*, *NCO*
		1173	Phenyl, *methyl*
#12	1122	1121	Phenyl, *methyl*, NCO
		1120	Phenyl, *methyl*, NCO
		1107	Phenyl, methyl
		1101	Phenyl, methyl
#13	1005	1004.1	Phenyl, *methyl*, *NCO*
		1004	
#14	927	930	Phenyl, methyl
		929	Phenyl, *methyl*
		927	Phenyl, methyl
		922	Phenyl, *methyl*
	903	902	Phenyl, methyl
#15	837	840	Phenyl, methyl, *NCO*
		831	
#16	798	807	Phenyl, methyl, *NCO*
		804	
		797	Phenyl, methyl, NCO
		796	
#17	738	738	Phenyl, methyl, NCO
	717	717	Phenyl, methyl, NCO
#18	678	689	Phenyl, methyl, *NCO*
		677	Phenyl, methyl, NCO

characteristic in the traditional sense (cf. Introduction) and they even localise for that spectral region of 4,4′-MDI but it has to be noted that the IR spectrum does not resolve each single eigenvibration. This loss of resolution is not only due to natural line broadening. It is also a consequence of almost equal frequencies for several normal modes. This observation applies for many other normal vibrations as well (cf. other spectral regions in Fig. 9).

In the region 2500–2100 cm^{-1} (Fig. 9b), the spectrum is dominated by one IR band - even the most intense in the whole spectrum that actually consists of two close-lying modes according to the symmetry reasons mentioned above. Fig. 10 illustrates the nature of these two modes with the help of vectors (arrows) showing the elongation of the atoms involved in these vibrations.

Both isocyanate groups are strongly involved in a kind of asymmetric bond stretching. Smaller displacements of the atoms in the phenylene rings contribute to both vibrations as well. Two modes are found because the isocyanates move either in-phase (2313 cm^{-1}) or anti-phase (2308 cm^{-1}). The in-phase mode possesses the smaller transition dipole moment and thus a weaker IR intensity than the anti-phase vibration (Fig. 9b). Spectra catalogues usually assign the IR band measured at 2280 cm^{-1} to the 'anti-symmetric stretching of the isocyanate group' (with ν_a(NCO) as common notation) thus pretending that there would be only one characteristic group frequency, i.e. one vibration, in that band. Moreover, this diction might associate a local mode for the NCO group but these vibrations are not localized at all.

The so-called fingerprint region (1700–650 cm^{-1}, Fig. 9c) convenes 42 normal vibrations that, again, cluster in many IR bands numbered from #4 to #18.

The normal modes in bands #4 to #8 involve various stretching vibrations of the phenylene rings but the vibrations are not well localized to these groups – cf. Fig. 11 for the normal modes at 1614 cm^{-1} and 1529 cm^{-1} as examples from IR bands #4 and #6, respectively.

The methylene and sometimes even the isocyanate group (e.g. in #6) contribute significantly to the vibration. Each of bands #4 - #6 is composed of an in-phase and an anti-phase vibration of the atomic groups with similar frequencies.

The calculated IR bands #7 – #18 show similar features as summarised in Table 4.

In conclusion, these findings for the 4,4′-MDI conformer **B** demonstrate that the classical group frequency concept in spectra catalogues does not apply to the majority of normal vibrations: Instead, they involve coupled elongations and deformations of a large part of the atoms of the molecule. The assignment of an IR band to an isolated local vibration of a cluster of few atoms is precarious for the interpretation of IR spectra.

As a next step, the mid-IR spectra for conformers **A**, **B**, **C**, as representatives of the conformer classes **I** – **III**, are depicted in Fig. 12. Direct comparison without normalization of spectral intensity is possible in this case since the three spectra were calculated by the same method. Moreover, we abstain from normalization as it may mask conformer specific differences. The spectra are very similar to each other. The corresponding

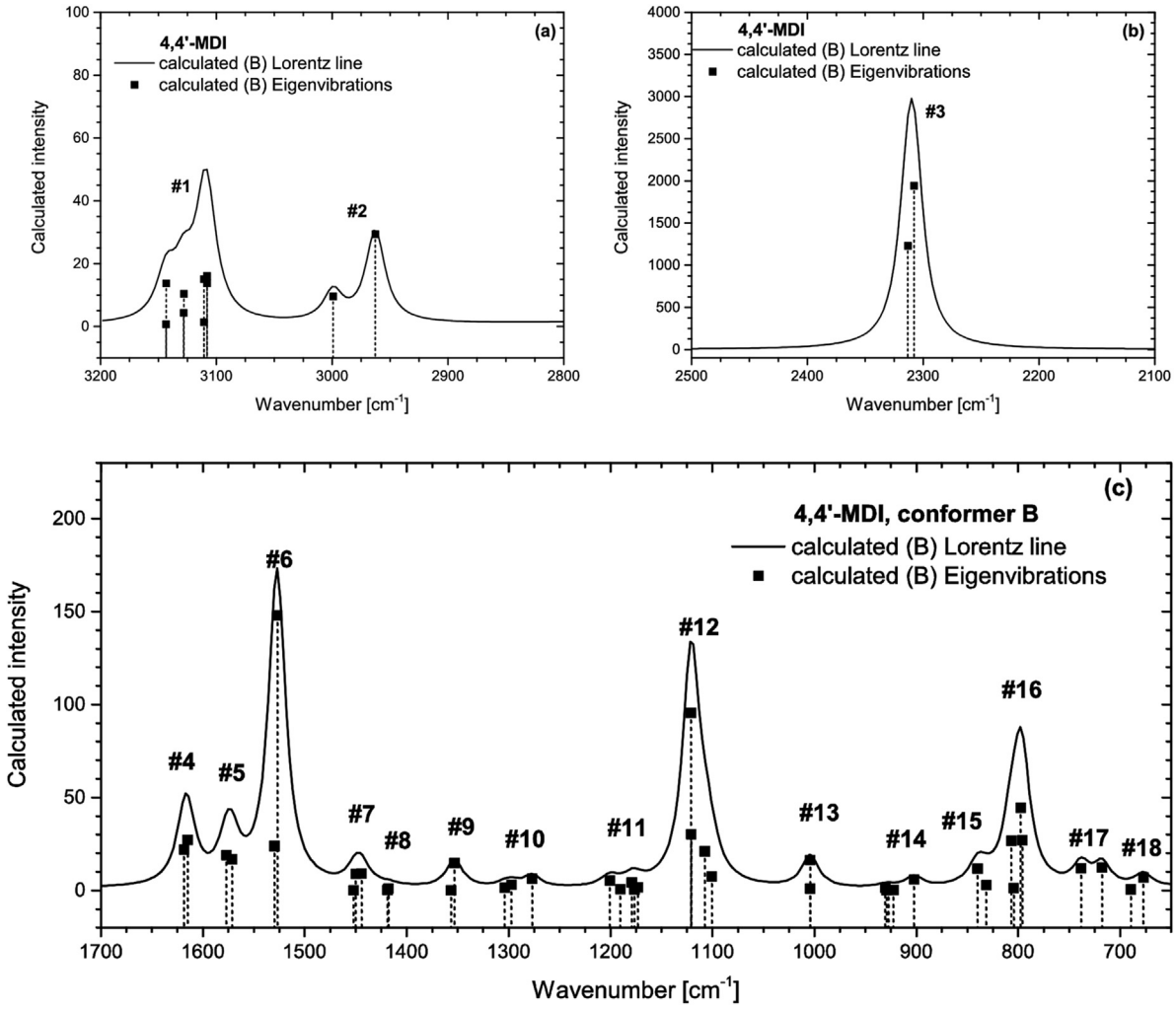

Fig. 9. Detailed view of the eigenvibrations (black squares on top of dotted lines) and calculated spectrum with Lorentzian line broadening (black line) for the conformer **B** of 4,4′-MDI. The prominent absorption bands are indexed from 1 to 18. Calculated intensity given in arbitrary units.

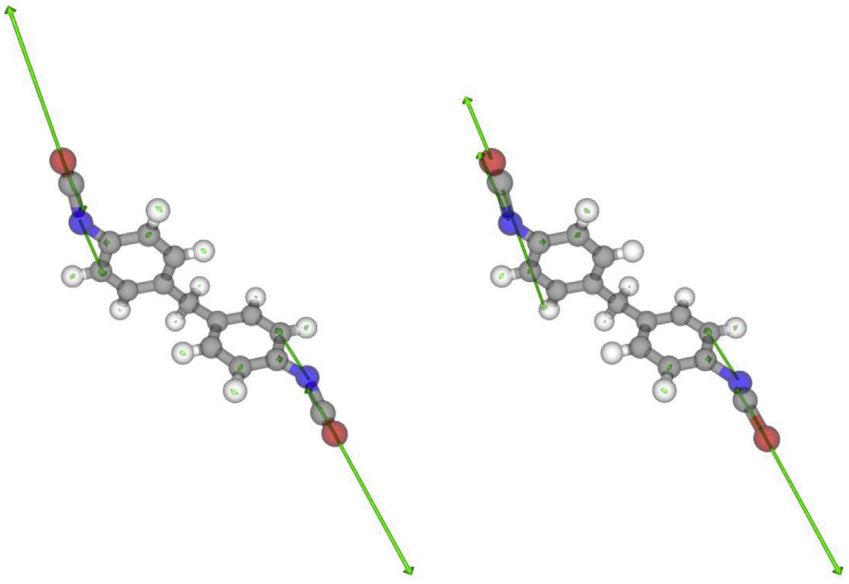

Fig. 10. Atom motions in the normal vibrations at 2313 cm^{-1} (left) and 2308 cm^{-1} (right) for conformer **B**. Arrows indicate the atom elongations.

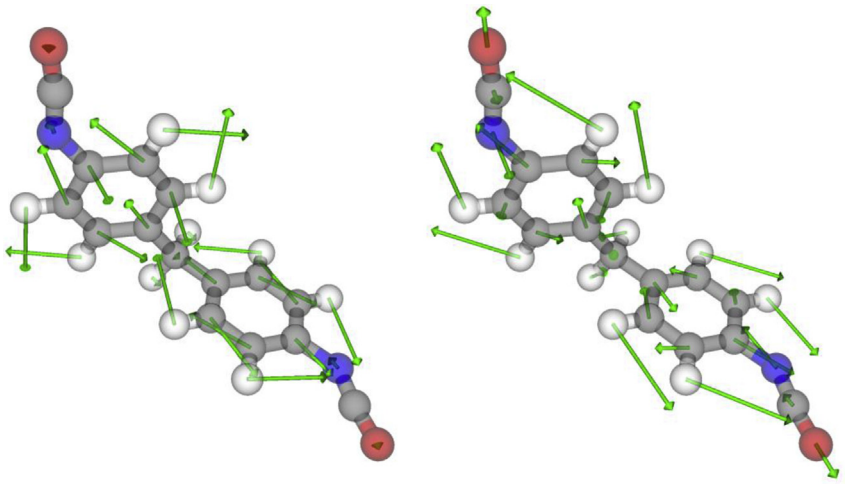

Fig. 11. Atomic motions in the normal vibrations of conformer **B** at 1614 cm^{-1} (left) in IR band #4 and 1529 cm^{-1} (right) in band #6 (cf. Fig. 9).

eigenvibrations appear at the same position or are shifted by only a few wavenumbers (1–3 cm^{-1}). For some bands (e.g. #2, #6, #7, #8, #11 and all bands between 1000 and 750 cm^{-1}), the calculated intensities of the eigenvibrations are identical for the three conformations. For the other bands, some differences in the intensity are present. For example the two eigenvibrations of NCO (#3, cf.

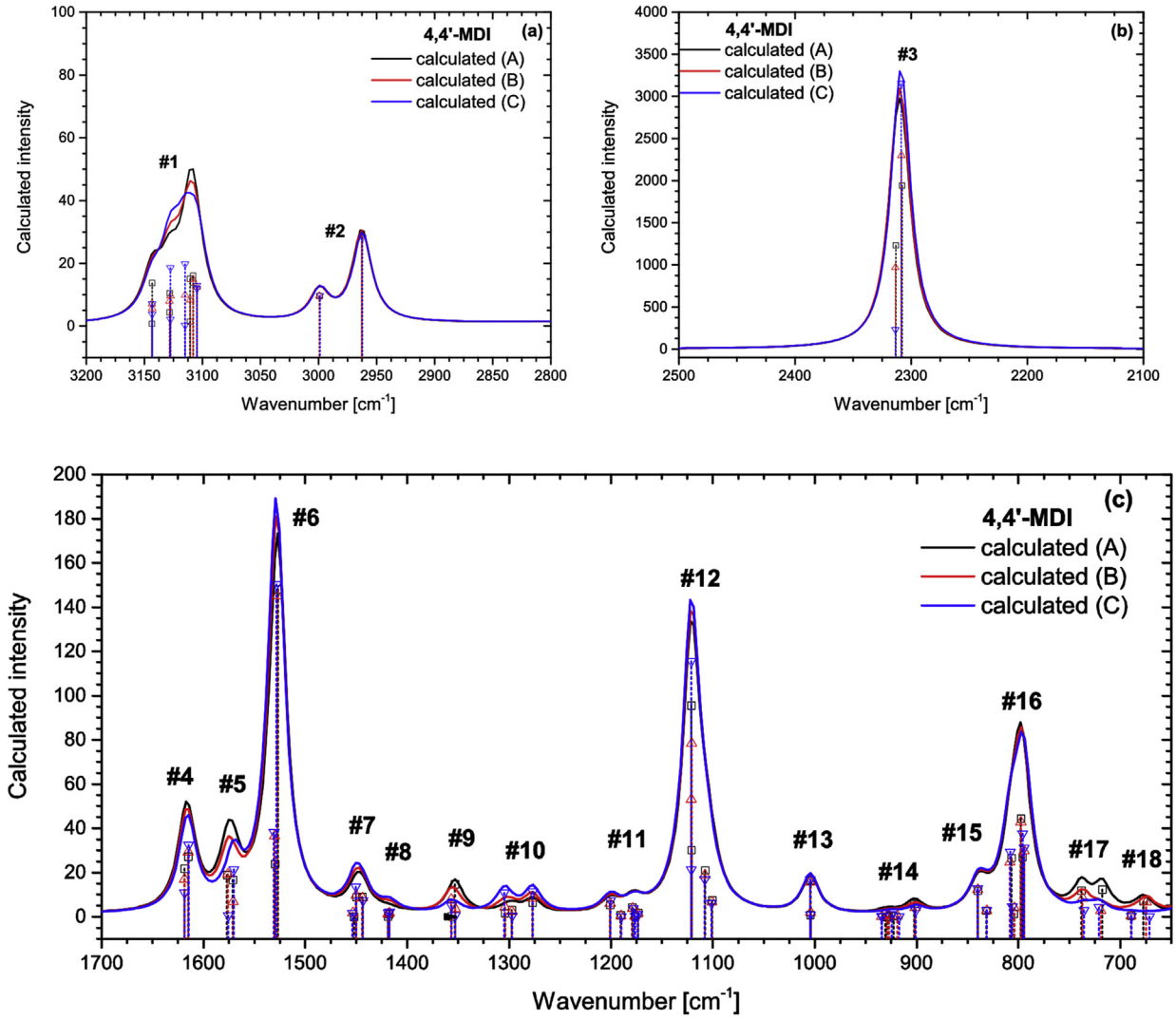

Fig. 12. The calculated spectra of three conformers: **A** (black), **B** (red) and **C** (blue). (For interpretation of the references to colour in this figure legend, the reader is referred to the web version of this article.)

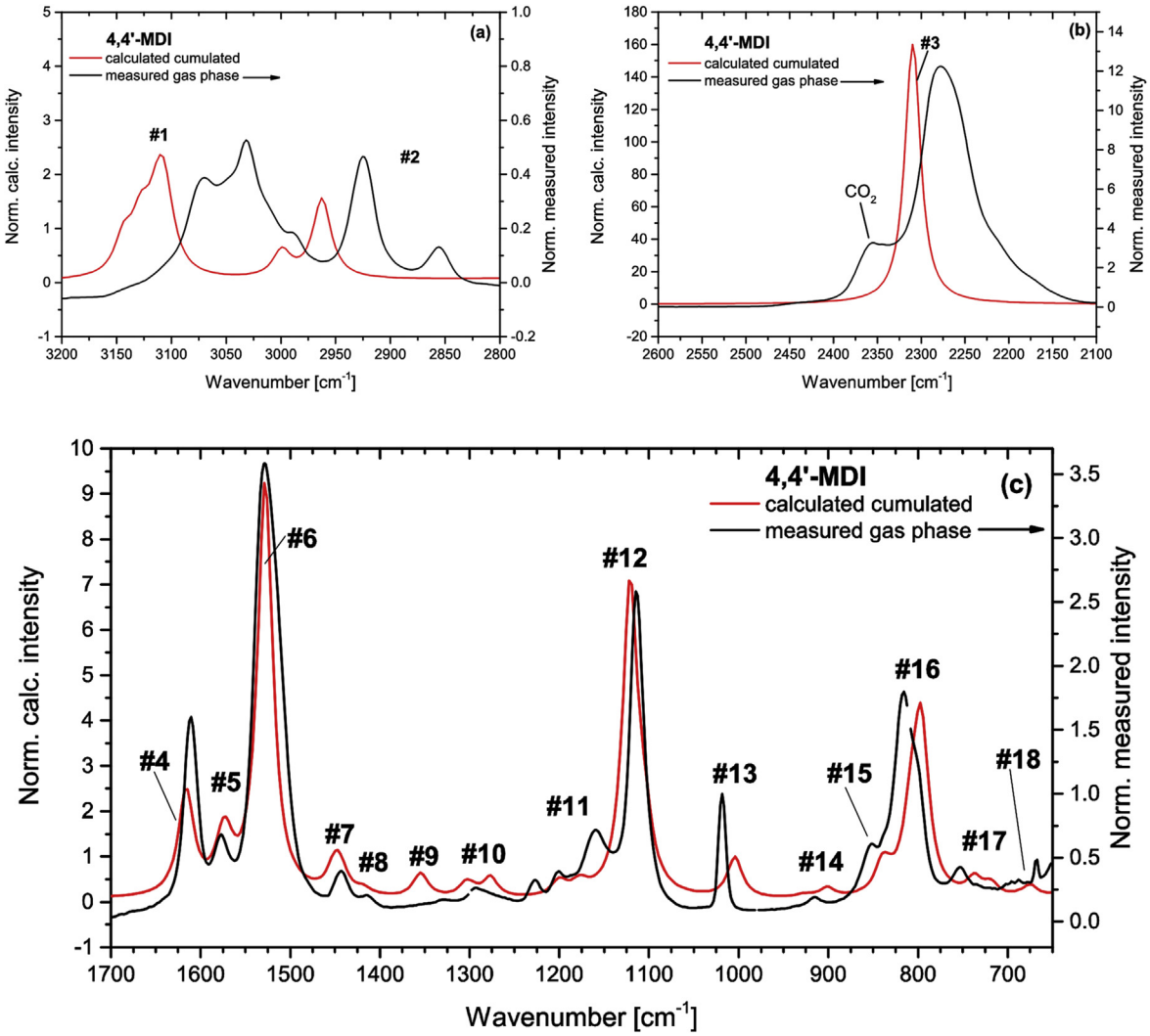

Fig. 13. Detailed views of the normalised cumulated spectrum for a 'conformation average' 4,4′-MDI molecule (red) and the normalised measured spectrum (black, normalised intensity given as '1-T') for gas phase 4,4′-MDI. Normalised intensities are scaled *differently in graphs a, b and c* to facilitate good visual comparability. The band at 2356 cm^{-1} in the experimental spectrum originates from residual CO_2 in the gas. (For interpretation of the references to colour in this figure legend, the reader is referred to the web version of this article.)

discussion above for the conformer **B**) are at the same positions (2313 cm^{-1}, 2308 cm^{-1}) in the conformers but the in-phase vibration intensities vary as $I_B > I_A > I_C$ while the anti-phase mode follows exactly the opposite trend. This explains why the overall intensity of the IR band #3 is almost the same for each conformer. The intensities of IR bands #1, #4, #5 and #12 are very similar for all conformers as well. The only remarkable difference of IR band intensities appears between 1350 − 1250 and 750–650 cm^{-1} where they obey $I_B > I_A > I_C$. Unfortunately, these spectral regions are of little value for diagnostics, cf. Table 4. Finally, the IR bands combine the same normal vibrations for the three conformers. Hence analyses similar to the one given in Table 4 for conformer **B** apply to conformers **A** and **C** as well.

In conclusion, the conformation state hardly influences the normal modes of 4,4′-MDI and the differences will not be distinguished in a measured IR spectrum. Nonetheless the calculated spectra have to be superimposed appropriately before comparing with the measured gas phase spectrum.

Therefore we simulate a reference spectrum for an experimental spectrum by adding the conformer IR spectra weighted with their cumulated probabilities given in Table 3. This cumulated spectrum represents the average over the conformations of a single 4,4′-MDI molecule. The intensity is normalised to the internal reference band #13 at about 1019 cm^{-1} again and given on the left ordinate. Fig. 12 proves the band #13 to be suitable for such purpose because it does not depend on the conformer state. Fig. 13 shows the cumulated spectrum in red in three spectral segments. The cumulation levels the small differences between the conformer spectra seen in Fig 12. Hence the IR band positions and intensities of an average 4,4′-MDI molecule are not sensitive to conformation.

Finally, the cumulated calculated IR spectrum is compared with the normalised spectrum measured for gaseous 4,4′-MDI (black spectrum in Fig. 13, normalised intensity given on the right ordinate). The two ordinates in Fig. 13 reveal strong discrepancies of measured and calculated spectra even for normalised intensities. This results from the well-known fact that the calculated intensities are related with considerable inaccuracies: They are related to the (square of the) change in the dipole moment due to the vibrational transition during light absorption, and this transition dipole moment is a quantity that only with extended basis sets can be calculated accurately. Another complication comes from the fact that the intensity of a measured transmittance spectrum scales

with the optical path length, z – cf. eqs. (4a), (7a). All these aspects make it difficult to obtain a quantitative agreement between experimental and theoretical spectra, even in terms of normalised intensity. Therefore, the only option left with spectral intensity is an evaluation of *height ratios of adjacent peaks* (e.g. in a doublet). These ratios in the calculated spectrum should compare with their counterparts in the gas spectrum.

The bands in the region 3200–2800 cm^{-1} (Fig. 13a) originate from CH stretching vibrations. Similar bands are observed in both spectra (triplet #1: aromatic C–H, doublet #2: methylene C–H) but the calculated ones are found at higher wavenumbers (the difference is roughly $\Delta\tilde{\nu} \approx 80–100\ cm^{-1}$). In the literature, such frequency shifts are reported as being typical for DFT-calculated spectra in this frequency region [18,19]. Moreover, the intensity ratios measured in the gas phase for triplet #1 and doublet #2 are inverse to the corresponding ratios in the cumulated spectrum. At the first glance, this deviation might also be attributed to the problems with the calculated intensities. However, these strongly modified intensity ratios *and* the above-mentioned presence of molecular interactions in the measured 4,4′-MDI gas support another reasonable suspicion: The calculated positions for the CH stretch vibrations might be not that bad. Their difference to the measured band positions might be at least in part due to the red shift expected for vibration frequencies in interacting molecules relative to those of an isolated molecule in vacuum.

The calculated isocyanate asymmetric stretching (Fig. 13b, at 2310 cm^{-1}) appears at 33 cm^{-1} above of the measured position (#3, 2277 cm^{-1}). Now, isocyanate groups are prone to interactions and the NCO band appears at the same position (within the limit of spectral resolution, cf. Fig. 3c) in both measured spectra (gas phase and liquid). That fact supports the conclusion that our gas spectrum depicts *interacting* 4,4′-MDI. Hence, the calculated eigenfrequency might again be close to the true value for a single 4,4′-MDI in vacuum rather than a numerical artefact.

The fingerprint region (1700–650 cm^{-1}, Fig. 13c) reveals more features. The positions of the measured and calculated bands #4 to #12 differ by < 20 cm^{-1} and nowhere else simulated and measured band positions agree better and this little deviation can be considered as the limit of accuracy. The peak ratios are fairly similar too. Both findings could suggest that, in this frequency range, the eigenvibrations are largely independent of molecular interactions. Provided we got intermolecular interactions in the gas phase, the two measured spectra support this idea as they are identical within the limits of experimental accuracy (cf. Fig. 3d). Moreover, more or less all atoms of the 4,4′-MDI molecule are involved in the vibrations in this spectral range and they superimpose to #4 - #12 in different manners (Table 3). Thus, bands #4 - #12 are not sensitive to molecular interactions.

Below 1050 cm^{-1}, we observe a strange type of disagreement: The calculated bands progressively shift to *lower* frequencies (energies) compared to the measured spectrum. This is in conflict with the idea that intermolecular interactions are responsible for the differences between simulation and experiment, since these interactions will always result in a reduction of the *measured* vibration frequency. Moreover, we do not see similar shifts in the measured spectra (Fig. 3d). The shift to lower frequency is, accordingly, attributed to a numerical artefact in the simulation algorithms.

4. Conclusions

The DFT calculation of the IR eigenfrequencies for the 4,4′-MDI molecule proves that the IR bands are not accurately assigned by using common band catalogues due to a number of reasons. As an alternative, a detailed assignment is presented for the IR-active eigenvibrations. The conformational study reveals that 4,4′-MDI possesses eight conformers. For symmetry reasons, the conformers group into three classes according to their properties. These classes mainly differ by the tilt of the phenylene rings and the orientation of the two NCO groups (cf. Fig. 7). The molecule's conformational energy landscape necessary to pass from one conformer to another was calculated. Of the two paths we considered, the most favourable way for conformational changes consists in rotating the phenylene ring plus the attached NCO group simultaneously while keeping the NCO in the plane of the phenylene ring. The energy differences of and the barriers between the conformers are sufficiently small to give a significant Boltzmann population for all of them.

The IR spectrum was calculated for each conformer, giving access to any eigenvibration of the isolated 4,4′-MDI molecule. Almost all modes involve motions of nearly all atoms. Many modes group together as they have only very little differences in the vibration frequency. That proves that the traditional group frequency concept has to be used with great care if at all. Real IR bands possess a natural line width described by a Lorentz line shape, and another line broadening effect due to molecular interactions which usually is summarised as impact broadening. For the 4,4′-MDI conformers, any IR band contains more than one of these broadened normal vibration modes. The calculated IR spectra of the four 4,4′-MDI conformers reveal only minor differences. Hence, the IR spectra are not sensitive to the different conformations of the 4,4′-MDI.

In order to compare with measured 4,4′-MDI IR spectra, the conformer IR spectra were weighted with the corresponding Boltzmann probabilities and superimposed. Such a comparison helps to assess the quality of this quantum-mechanical study. As the interaction of infrared light with molecules is not accurately described using DFT, the absolute as well as the normalised intensity of the individual IR bands is not reliable. A comparison of normalised intensity *ratios* is though possible to some extent. In the region of CH and isocyanate stretch modes (3200–2000 cm^{-1}), the calculated bands are found at higher wavenumbers than in the measured spectrum and the intensity ratios differ from the measured ones. In part, this will originate from the approximate DFT functional but we have to recall that the simulation only considers an isolated molecule in vacuum. In real samples in gas or liquid phases, molecules interact. We showed that molecular interactions affect the liquid *and* gas phase IR spectra of 4,4′-MDI as well. Hence, part of the ‘red shift’ of the measured bands with respect to the calculated ones could be due to molecular interactions. This interesting point is left for future studies.

In the fingerprint region (1700 - 1050 cm^{-1}), the band positions and normalised intensity ratios are reproduced by the calculations. Hence, as these bands involve all atoms in different combinations, the influence of the intermolecular interactions is widely cancelled out here.

Below 1050 cm^{-1}, numerical artefacts from the DFT calculation shift the calculated spectrum to lower wavenumbers.

Despite these differences between experimental and calculated spectra, an accurate band assignment, indicating how the atoms of the molecule are involved in each IR band, is now available for the 4,4′-MDI molecule. This finding will form the basis for future studies where the changes in the spectra are to be investigated experimentally and theoretically when the molecule is deposited on native metal surfaces. Such effort will give information on the structure of the surfaces and on the bonding between surface and molecule.

Acknowledgment

The work was kindly supported by German DFG (PO 577/23-1,

Sp 437/33-1) and by the National Research Fund, Luxembourg within the projects (3907394) and (1186539). The authors owe thanks to Max Ramirez for his contribution on the development and testing of the adequate calculation algorithms for this study. We are grateful for the provided computational resources within the C^3MSaar.

References

[1] D. Lin-Vien, N.B. Colthup, W.G. Fateley, J.G. Grasselli, The Handbook of Infrared and Raman Characteristic Frequencies of Organic Molecules, Academic Press, Boston, 1991.
[2] N.P.G. Roeges, A Guide to the Complete Interpretation of Infrared Spectra of Organic Structures, John Wiley & Sons, Chichester, 1994.
[3] B. Smith, Infrared Spectral Interpretation - a Systematic Approach, CRC Press, Boca Raton, 1999.
[4] G. Socrates, Infrared Characteristic Group Frequencies - Tables and Charts, second ed., John Wiley & Sons, Chichester, 1994.
[5] H. Günzler, A. Williams, Handbook of Analytical Techniques, Wiley-VCH, Weinheim, Germany, 2001.
[6] V. Hopfe, P. Klobes, W. Grählert, FSOS—Softwaresystem for the calculation of IR–VIS–UV–spectra of solids, thin layers and surfaces, in: Fraunhofer Institut für Werkstoffphysik und Schichttechnologie, Dresden, Germany, 1996.
[7] C. Wehlack, Chemische Struktur und ihre Entstehung in dünnen Epoxid- und Polyurethanschichten auf Metallen, in: Saarbrücker Reihe Materialwissenschaft und Werkstofftechnik, 14, Shaker Verlag, Aachen, Germany, 2009.
[8] C. Nies, C. Wehlack, H. Ehbing, D.J. Dijkstra, W. Possart, J. Adhes. 88 (2012) 665–683.
[9] C. Wehlack, W. Possart, Macromol. Symp. 205 (2004) 251–261.
[10] C. Nies, F. Fug, C. Otto, W. Possart, Int. J. Adhes. Adhes. 52 (2014) 19–25.
[11] M.J. Frisch, G.W. Trucks, H.B. Schlegel, G.E. Scuseria, M.A. Robb, J.R. Cheeseman, G. Scalmani, V. Barone, B. Mennucci, B.A. Petersson, et al., Gaussian, Inc., Wallingford, CT, 2010.
[12] C. Lee, W. Yang, R.G. Parr, Phys. Rev. B 37 (1988) 785–789.
[13] A.D. Becke, J. Chem. Phys. 98 (1993) 5648–5652.
[14] J.P. Perdew, K. Burke, M. Ernzerhof, Phys. Rev. Lett. 77 (1996) 3865–3868.
[15] R.S. Stein, J. Powers, Topics in Polymer Physics, Imperial College Press, London, 2006.
[16] M.B. Jackson, Molecular and Cellular Biophysics, Cambridge University Press, Cambridge, 2006.
[17] E.Z. Zhuravlev, P.V. Mulyanov, N.M. Moncharzh, Zh Obshchei Khim 45 (1975) 1605–1610.
[18] C. Adamo, V. Barone, J. Chem. Phys. 108 (1998) 664–675.
[19] A. Gorski, S. Gawinkowski, J. Herbich, O. Krauss, B. Brutschy, R.P. Thummel, J. Waluk, J. Phys. Chem. A 116 (2012) 11973–11986.